

Nonuniform-temperature effects on the QCD phase transition

Jun-Hui Zheng and Lijia Jiang

Center for Quantum Spintronics, Department of Physics,
Norwegian University of Science and Technology, NO-7491 Trondheim, Norway

We study the phase transition in a steady temperature-nonuniform system in the frame of the Ising model. We calculate the nonuniform-temperature effects on the phase transition point, the fluctuations, and the correlation length of the order parameter. We find the phase transition could happen at a temperature higher than the equilibrium phase transition temperature of a temperature-uniform system. Besides, the fluctuations and the correlation length are enhanced near the phase transition point, and they monotonously increase from the crossover regime to the first order phase transition regime without exotic behavior at the critical point. Our study is helpful to understand the behaviors of QCD phase transition in the relativistic heavy-ion collision and provides a method to evaluate the nonuniform-temperature effects for the order parameter.

INTRODUCTION

Exploring the QCD phase boundary and critical point (CP) is one of the main goals in relativistic heavy-ion collision (RHIC) experiments [1–5]. In the collider, a fireball quickly forms and cools down continuously. During the fireball’s expansion, the QCD matter cools from the quark-gluon-plasma (QGP) phase to the hadronic phase. A dynamical phase transition (PT) surface exists in the fireball, which separates the two phases [6–10]. The hadrons and resonances outside the surface collide with each other and part of them decay. A hypersurface named chemical freeze-out surface subsequently coexists outside the dynamical PT surface, where the inelastic collision between the hadronic matter ceases [11].

Searching the phase boundary and the CP from the dynamical process in RHICs, we have to face two fundamental questions. Does the dynamical PT boundary coincide with the equilibrium PT boundary in the QCD phase diagram? Are the critical behaviors kept to identify the CP?

Recent studies show that the chemical freeze-out line fitted from experimental data overlaps with the equilibrium PT boundary depicted by the lattice calculations [12–19]. It strongly hints the dynamical PT inside the fireball happens at a temperature above the equilibrium PT temperature (see the sketch of an instantaneous fireball in Fig. 1). This is in contrast to the dynamical delay effects in a temperature-uniform system, where the dynamical PT follows and memorizes the behaviors of equilibrium PT [20–24]. On the other hand, the fluctuations and correlation length of the QCD order parameter (i.e., the σ field) have been broadly used to discuss the fluctuation behaviors of observables such as net charge, baryon number and particle ratios, etc [4, 5, 25, 26]. The correlation length has been estimated by including the finite size effect and the critical slowing down effect [20, 27]. Yet it is still unclear what are the behaviors of the fluctuations and correlation length near the CP in a finite-size system with nonuniform temperature.

In this article, we pursue to discuss the relation between the dynamical and the equilibrium PT surface in the fireball, by studying the behaviors of the QCD order parameter field in spatially-nonuniform-temperature profiles near the dynamical

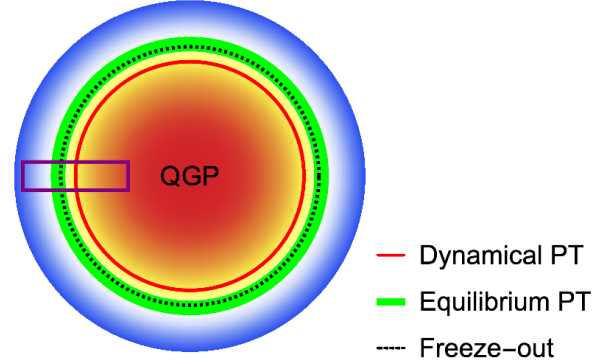


FIG. 1. A sketch of an instantaneous fireball. The temperature decreases from inner to outer (red to blue). The red solid circle represents the dynamical phase transition (PT) surface. The black dashed line is the chemical freeze-out surface. The green brush line refers to the isothermal surface of the equilibrium PT temperature in temperature-uniform systems.

PT surface. As both the position and the shape of the dynamical PT surface vary with time during the fireball evolution, we look into the σ field in the comoving frame of the PT region. As shown in Fig. 1, we take an instantaneous slender brick cell in the fireball with the dynamical and equilibrium phase boundary located in the middle. In this brick cell, the temperature is spatially nonuniform. We further suppose the relaxation of the σ field configurations in the brick cell at various time approaches to zero. Thus, the σ field reaches the thermal equilibrium distribution instantly. With this Markov assumption, the instantaneous dynamical PT surface turns into the stationary PT surface in a nonuniform-temperature system.

By mapping the QCD effective potential to the Ising model, we illustrate that the PT temperature in a temperature-nonuniform system could be above the equilibrium PT temperature T_c of a temperature-uniform system. It hints a possibility that hadrons form before the QGP cools down to T_c during the fireball evolution. We further deduce and discuss the fluctuation strength and the correlation length of the σ field in the PT region, and find that the CP presents no typical critical behaviors compared to the other PT scenarios. At the same time, the fluctuations and the correlation length in the

PT region is significantly increased compared to that in the periphery of the cell.

TEMPERATURE PROFILE

First, we formalize the temperature profile in the brick cell. For simplicity, we suppose the y - z plane is isothermal, and the temperature function along the x -axis is spatially dependent,

$$T(x) = T_c + \frac{\delta T}{2} \tanh\left(\frac{x}{w}\right), \quad (1)$$

where δT is the temperature bias between the two ends of the cell and the width w dominates the range of the region near the equilibrium PT surface where a finite temperature gradient ($\sim \delta T/2w$) presents. Note that the real temperature profile is determined by the background matter fields (hadrons, quarks and gluons) [28]. An example with a more realistic temperature profile is present in the appendix, the results qualitatively agree with that from the tanh-type temperature profile. However, due to the complexities of the RHIC (chemical potential, viscosity etc.), we adopt this simplified tanh-type profile, and focus our attention mainly on the nonuniform-temperature effects in the PT region. In the following, we will also assume the baryon chemical potential is homogeneous in the cell.

PARTITION FUNCTION

As the local equilibrium assumption in relativistic hydrodynamics is proved to be well-performed [28–33], we carry on this assumption in our calculation. Thus, the partition function of the system is a product of the local partition function of the σ field at different x . In the continuous limit, we have

$$\mathcal{Z}[\sigma] = \int \mathcal{D}\sigma P[\sigma], \quad (2)$$

where the weight function is

$$P[\sigma] = \exp\left\{-\int d\mathbf{r} \frac{(\nabla\sigma)^2/2 + V[\sigma(\mathbf{r})]}{T(x)}\right\}, \quad (3)$$

with $\mathbf{r} = (x, y, z)$. The effective potential of the σ field can be obtained from the QCD-inspired models [17, 34–40]. As we mainly focus on the regime near the CP, we parameterize the potential by analogy to the Ising model. In the simplest Ising mapping [41–43], we have

$$V[\sigma] = a(T - T_c)(\sigma - \sigma_0) + b(\mu - \mu_c)(\sigma - \sigma_0)^2 + c(\sigma - \sigma_0)^4, \quad (4)$$

where $a > 0$, $b < 0$ and $c > 0$ are parameters which depend on the real effective potential, (μ_c, T_c) marks the position of the equilibrium CP. Note that within this mapping, the PT temperature is μ independent. For $\Delta\mu \equiv \mu - \mu_c > 0$ and $\Delta\mu < 0$, the effective potential describes the first order PT and crossover respectively as the change of temperature. σ_0 (about 45 MeV)

is introduced to shift the σ field to the realistic values. Since the value of σ_0 will not influence our discussion on fluctuations and correlation length, we simply set $\sigma_0 = 0$ in the following. Then, in thermal equilibrium, $\sigma < 0$ and $\sigma > 0$ correspond to the QGP phase and the hadron phase, respectively.

Throughout the article, we set the parameters $a = 0.5 \text{ fm}^{-2}$, $b = -0.25 \text{ fm}^{-1}$, and $c = 3.6$ to simulate the effective potential from the linear sigma model [37, 38]. The PT temperature $T_c = 160 \text{ MeV}$ is chosen from the result of lattice simulations [17, 18]. For the temperature profile, the temperature bias is set as $\delta T = 40 \text{ MeV}$ and the width is set to be $w = 1 \text{ fm}$ (or $w = 0.5 \text{ fm}$). Then the temperature gradient is 20 MeV/fm (40 MeV/fm), corresponding to the mean temperature gradient in a fireball of radius 10 fm with the central temperature being 200 MeV (400 MeV).

THE ORDER PARAMETER PROFILE

Since the temperature is spatially nonuniform, the local order parameter which maximizes the weight function is never again determined by minimizing the effective potential $\partial V[\sigma]/\partial\sigma = 0$, but satisfies the extreme value condition of the weight function, $\delta P[\sigma]/\delta\sigma = 0$. Explicitly, we have

$$\nabla^2\sigma = \frac{1}{T} \nabla T \cdot \nabla\sigma + \frac{\delta V}{\delta\sigma}. \quad (5)$$

As we suppose the temperature distribution in the y - z plane is isothermal, the $\sigma(\mathbf{r})$ that maximizes the weight function must be flat in this plane. Thus $\sigma(\mathbf{r})$ depends only on x , and Eq. (5) reduces to a one-dimensional problem. The boundary condition is given by the local order parameters at the ends, i.e., $\sigma(x = -L/2) = \sigma_L$ and $\sigma(x = L/2) = \sigma_R$, where σ_L and σ_R are the global minimum point of the potential $V[\sigma]$ at $x = \mp L/2$ and L is the cell's length. Note that when L is sufficient large, i.e., $L \gg w$, the magnitude of L will not influence the following results.

The solution $\sigma_c(x)$ to Eq. (5) is presented in Fig. 2, with $w = 1 \text{ fm}$ and different $\Delta\mu$. A main information from these order parameter profiles is that $\sigma_c(x)$ changes its sign at $x > 0$, no matter the sign and magnitude of $\Delta\mu$. It is easy to check that, without the temperature gradient term $(1/T)\nabla T \cdot \nabla\sigma$, the solution $\sigma_c(x)$ is an odd function of x and vanishes at $x = 0$. As the $(1/T)\nabla T \cdot \nabla\sigma$ term is always negative ($\partial_x\sigma < 0$ and $\partial_x T > 0$), it will always contribute similar corrections to the solution $\sigma_c(x)$, and the sign change of $\sigma_c(x)$ will universally happens at $x > 0$. This result can be comprehended directly from the weight function Eq. (3). In the brick cell, the hot part with high temperature is more easily fluctuated than the cold part. Therefore, $\sigma_c(x)$ will tend to the order parameter value of the cold part, and $\sigma_c(0)$ becomes positive.

Like as the equilibrium PT of the Ising model, we identify the point of sign change of σ_c as the PT point at different $\Delta\mu$. The PT point always locates at $x > 0$ and the corresponding PT temperature is generally higher than the equilibrium PT

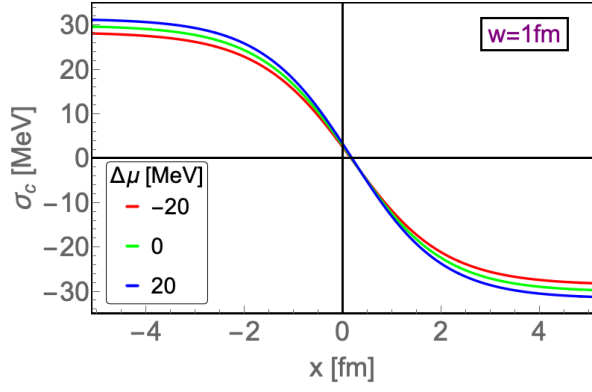


FIG. 2. The order parameter profile $\sigma_c(x)$ in the brick cell, with the red, green and blue lines represent results in the crossover ($\Delta\mu < 0$), CP ($\Delta\mu = 0$) and the first order PT ($\Delta\mu > 0$) scenarios, respectively.

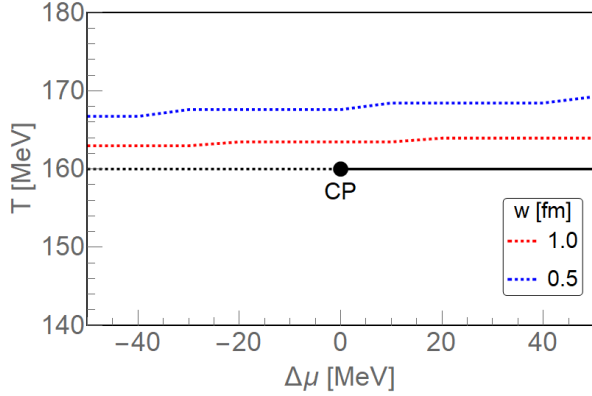


FIG. 3. A comparison of the PT temperature in the temperature-nonuniform (red and blue dotted lines) and temperature-uniform systems (black lines). The red dotted line is with $w = 1.0$ fm, and the blue dotted line is with $w = 0.5$ fm.

temperature $T_c = T(x = 0)$. The PT temperature can be evaluated from the temperature profile. In Fig. 3, we show the PT temperature for the two widths $w = 1$ fm and $w = 0.5$ fm. The PT temperature is lifted about 3 MeV and 8 MeV from T_c .

Note that the lifted values of temperature is not universal and depends on the temperature profile. In the RHIC, the temperature profile usually is not a tanh-type in the space. However, the PT point in a temperature-nonuniform system is generally different from that in a temperature-uniform system. The nonuniform-temperature effects provide a possibility that the QCD PT could happen before it cools down to T_c . In the appendix we present the result with a more realistic temperature profile fitted from the hydrodynamics' output. The PT temperature is also lifted, which qualitatively agrees with that from the tanh-type temperature profile. In the following, we keep our discussion on the tanh-type profile and reveal how the temperature profile influences the fluctuations and correlation length.

THERMAL FLUCTUATIONS

The fluctuations of the σ field are also changed by the temperature profile. We expand the σ field around the variational extremum solution with a small fluctuation, $\sigma(\mathbf{r}) = \sigma_c(x) + \delta\sigma(\mathbf{r})$. The weight function $P[\sigma]$ becomes

$$P[\sigma] = \exp \left[- \int d\mathbf{r} \frac{(\nabla\delta\sigma)^2/2 + m^2\delta\sigma^2/2 + 4c\sigma_c\delta\sigma^3 + c\delta\sigma^4}{T(x)} \right], \quad (6)$$

where the mass term $m^2(x) = 2b\Delta\mu + 12c\sigma_c^2$ is spatially dependent. In the following, we mainly focus on the variance of the fluctuations, so we omit the cubic and quartic terms which are related to the higher order fluctuations [25, 44, 45].

Conventionally, we start the discussion from the mass term of the $\delta\sigma$ field. In a temperature-uniform system, the mass term relates to the correlation length: $\xi = 1/m$. In the nonuniform case, we follow the old way and define a local correlation length: $\xi_{local}(x) = 1/\sqrt{m^2(x)}$. We present the results of $m^2(x)$ in the brick cell in Fig. 4. In the periphery, $m^2 \approx 1 \text{ fm}^{-2}$ corresponds to $\xi_{local} \approx 1 \text{ fm}$, which coincides with ξ since the temperature becomes flat apart from the center. In the central part, $m^2(x)$ presents exotic behaviors for different PT scenarios. In the crossover regime ($\Delta\mu < 0$), $m^2(x) > 0$ everywhere. For the critical value ($\Delta\mu = 0$), $m^2(x)$ vanishes at $\sigma_c = 0$, and the local correlation length ξ_{local} diverges. However, in the first order PT regime ($\Delta\mu > 0$), $m^2(x)$ is negative near the point $\sigma_c = 0$, which is in contrast with the positive m^2 in a temperature-uniform system. Therefore, the current definition of the local correlation length is not appropriate in the PT region with a finite temperature gradient. As we will show below, the variance of the local fluctuation $\delta\sigma(x)$ is always positive, and is better-suited to the description of the temperature-nonuniform system.

In the following, we calculate the variance of the fluctuation. We presume the size along the y and z direction is much smaller than the unknown correlation length. Therefore, we adopt the zero-mode approximation for y and z directions and thus $\delta\sigma(\mathbf{r})$ depends only on x . The cross-section of the brick cell is denoted as S . Discretizing the x -axis with spacing length Δx , the weight function becomes

$$P[\sigma] \approx \exp \left\{ - \frac{S}{2} \sum_{i,j} \delta\sigma_i M_{ij} \delta\sigma_j \right\}, \quad (7)$$

where the nonzero elements of the matrix M are

$$M_{ii} = \frac{1}{\Delta x} \left[\frac{1}{T_{i-1/2}} + \frac{1}{T_{i+1/2}} \right] + \frac{m_i^2 \Delta x}{T_i}, \quad (8)$$

$$M_{i,i+1} = M_{i+1,i} = - \frac{1}{T_{i+1/2} \Delta x}. \quad (9)$$

Here, ' i ' refers to the position $x = i\Delta x$. The matrix M must be positive definite so that the solution σ_c maximizes the weight function. We would like to emphasize the necessity and importance of the kinetic energy in $P[\sigma]$ (see Eq. (6)), which is

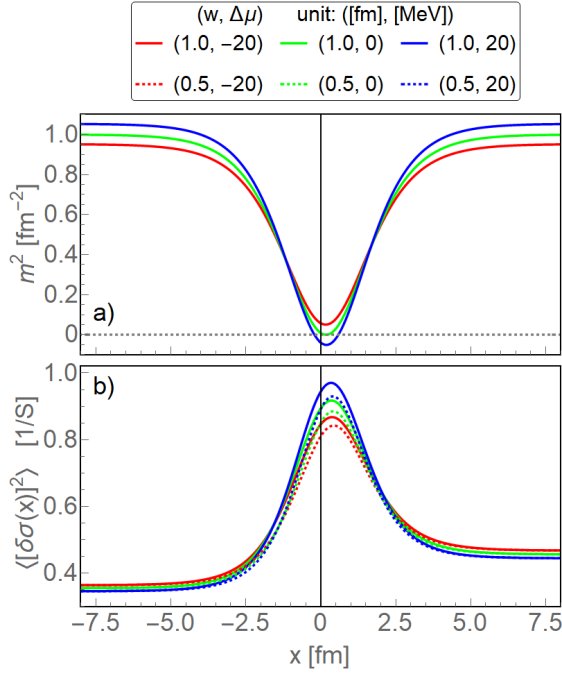


FIG. 4. Panel a) presents the local mass square of the fluctuating σ field, and panel b) presents the variance for different w and $\Delta\mu$. In both panels, the red, green and blue lines represents results in the crossover ($\Delta\mu < 0$), CP ($\Delta\mu = 0$) and the first order PT ($\Delta\mu > 0$) scenarios, respectively. Solid lines are results with $w = 1$ fm, and dotted lines are results with $w = 0.5$ fm.

finite and solves the negative $m^2(x)$ problem in the first order PT scenario. This is because in the brick cell, $m^2(x)$ constructs a potential well as shown in Fig. 4, and the kinetic term has to be finite due to the uncertainty principle. From the same reason, at $\Delta\mu = 0$, the fluctuations on the CP is not divergent due to a positive ground energy of M . The nonzero kinetic energy represents the contribution from the nonzero-mode fluctuation of the σ -field, which plays a crucial role in the temperature-nonuniform system.

The variance of the local fluctuations is

$$\langle [\delta\sigma_i]^2 \rangle = \frac{[M^{-1}]_{ii}}{S}. \quad (10)$$

In Fig. 4, we plot the results of the variance for different w and $\Delta\mu$. Note that the maximum point of the variance locates a little right of the minimum point of $m^2(x)$, because the fluctuations in the right of the cell is lifted due to a higher temperature compared to the left. Interestingly, the fluctuations on the PT point monotonically increase from the crossover ($\Delta\mu < 0$) to the first order PT ($\Delta\mu > 0$). There are no exotic behaviors to characterize the CP ($\Delta\mu = 0$). In addition, the fluctuations near the PT point are enhanced as the increase of the width w for all the three scenarios. This can be understood in the extreme case that $w \rightarrow \infty$, the temperature becomes flat locally and the fluctuations near the CP become divergent.

We further calculate the correlation length near the PT point

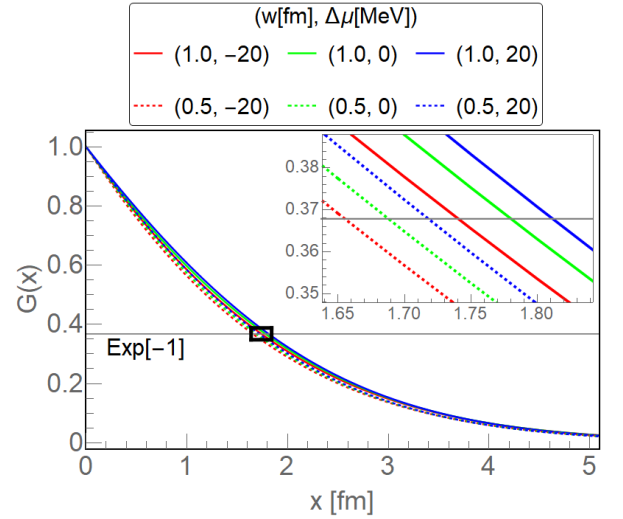


FIG. 5. The normalized nonlocal correlation $G(x)$ near the PT point. The legends are the same as that in Fig. 4. The inset is an enlargement of the cross region marked in the plot.

from the normalized nonlocal correlation,

$$G(x) = \frac{\langle \delta\sigma(x_p + x/2) \delta\sigma(x_p - x/2) \rangle}{\langle \delta\sigma(x_p) \delta\sigma(x_p) \rangle}, \quad (11)$$

where x_p denotes the spatial location of the maximum point of the variance. We plot the result in Fig. 5. The normalized nonlocal correlation doesn't exactly decay exponentially, so we determine the correlation length ξ by requiring $G(\xi) = \exp(-1)$. The ξ again smoothly increases from the crossover regime ($\Delta\mu < 0$) to the first order phase transition regime ($\Delta\mu > 0$), and decreases as the increase of the temperature gradient. With the current parameter set, our estimation of the correlation length is $\xi \approx 1.74$ fm in the central part of the brick cell, which is significantly larger than $\xi \approx 1$ fm in the periphery.

CONCLUSION AND DISCUSSION

We have developed a method to figure out the stablest order parameter profile, the fluctuations and the correlation length in a steady temperature-nonuniform system. We find that the PT temperature is generally ahead for different temperature gradients in our temperature profile settings. This hints a possibility that, in the Markov approximation, the hadrons may form before QGP cools to the equilibrium PT temperature during the fireball expansion. In addition, both the fluctuations and the correlation length near the PT surface are enhanced, and decrease as the increase of temperature gradient. There is no critical behavior to identify the CP from the first order PT and crossover.

In the RHIC, the realistic temperature profile as well as the baryon chemical potential profile vary for different events at different time, and they are affected by dynamical factors like

the viscosity. Even in the Markov approximation, statistical average over fluctuations in different profiles is needed. We expect the statistical average will not change our results qualitatively.

Our study provides a different perspective to understand the QCD PT in RHIC. Indeed, the nonuniform-temperature effects and the dynamical memory effects [21, 43, 46–52] are two extreme cases corresponding to spatial correlation dominant and temporal correlation dominant, respectively. During the dynamical evolution of the fireball, the two effects may interrelate with each other. In our calculation for a steady nonuniform-temperature system, the correlation length near the PT surface increases significantly. Consequently, in the dynamical evolution, the slowing down of dynamics is expected in all the PT regime and the memory effects will be enhanced. Regarding the current measurements on the fluctuations of net proton [4, 5], the nonuniform-temperature effects on the high order fluctuations should be studied, and we believe a combination of the nonuniform-temperature effects and the dynamical effects will provide a better description to the PT in RHIC.

This work was supported by the Research Council of Norway through its Centres of Excellence funding scheme (project no. 262633, “QuSpin”). Lijia Jiang thanks Xiaofeng Luo and Bao-Chi Fu for helpful discussions.

APPENDIX

In this Appendix, we show an example with a more realistic temperature profile as show in Fig. 6. Here, $T(x = 0) = T_c$ is the phase transition temperature. The position $x = 5$ fm locates in the center of the fireball and the position $x = -5$ fm is the left boundary of the fireball. We keep all the other parameter sets unchanged, and assume the effective potential (Eq. (4) in the main text) is valid in the whole temperature region. The corresponding extreme solution $\sigma_c(x)$ is shown in Fig. 7. In this plot, the phase transition happens at $x > 0$, where $T \approx 168$ MeV is 8 MeV larger than T_c .

In Fig. 8, we show the results of local mass square and the variance of the fluctuations. The local correlation lengths ($1/m$) at $x = \pm 5$ fm are $\xi_{local} \approx 0.73$ fm and 0.5 fm, respectively. The variance vanishes at $x = -5$ fm since $T \rightarrow 0$. In Fig. 9, the normalized nonlocal correlation near the PT point is plotted. The correlation length is about 1.45 fm. The variance and correlation length with this temperature profile present similar behaviors as those in the main text.

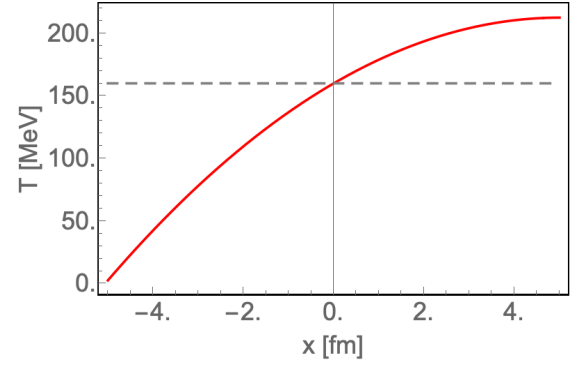


FIG. 6. The temperature profile in the real space. Here, for $x = 0$, $T = T_c$. The position $x = 5$ fm locates in the center of the fireball and the position $x = -5$ fm is the left boundary of the fireball.

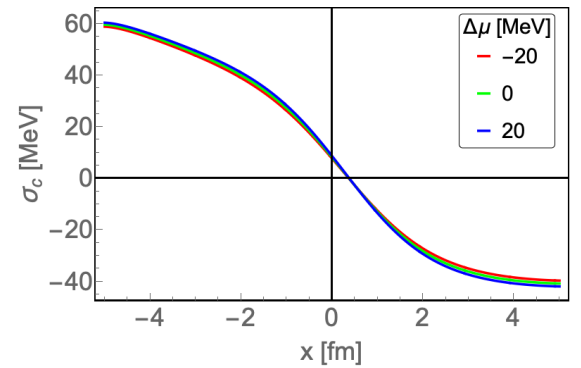


FIG. 7. The order parameter profile $\sigma_c(x)$, with the red, green and blue lines represent results in the crossover ($\Delta\mu < 0$), CP ($\Delta\mu = 0$) and the first order PT ($\Delta\mu > 0$) scenarios, respectively.

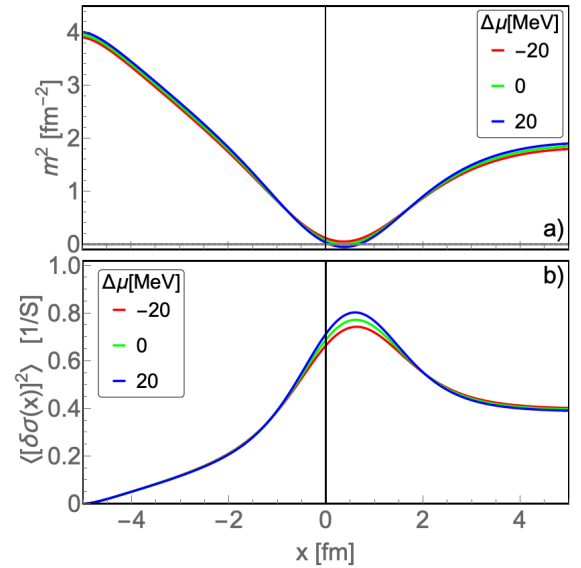


FIG. 8. Panel a) and b) present the local mass square and the variance of the fluctuating σ field, respectively. In both panels, the red, green and blue lines represents results in the crossover ($\Delta\mu < 0$), CP ($\Delta\mu = 0$) and the first order PT ($\Delta\mu > 0$) scenarios, respectively.

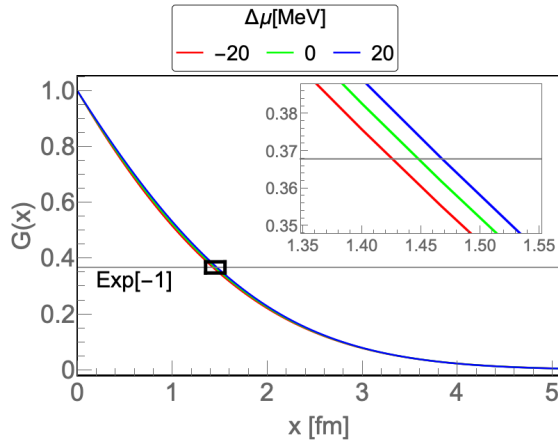


FIG. 9. The normalized nonlocal correlation $G(x)$ near the PT point. The inset is an enlargement of the cross region marked in the plot.

- [1] M. M. Aggarwal et al. (STAR), (2010), [arXiv:1007.2613 \[nucl-ex\]](#).
- [2] [BES-II White Paper \(STAR Note 2014\)](#).
- [3] W. Busza, K. Rajagopal, and W. van der Schee, *Annual Review of Nuclear and Particle Science* **68**, 339 (2018), <https://doi.org/10.1146/annurev-nucl-101917-020852>.
- [4] J. Adam et al. (STAR), (2020), [arXiv:2001.02852 \[nucl-ex\]](#).
- [5] M. Abdallah et al. (STAR), (2021), [arXiv:2101.12413 \[nucl-ex\]](#).
- [6] J. Letessier and J. Rafelski, *Hadrons and Quark-Gluon Plasma*, Cambridge Monographs on Particle Physics, Nuclear Physics and Cosmology (Cambridge University Press, 2002).
- [7] Y. Aoki, G. Endrődi, Z. Fodor, S. D. Katz, and K. K. Szabó, *Nature* **443**, 675 (2006).
- [8] A. Bazavov et al. (HotQCD), *Phys. Rev. D* **85**, 054503 (2012).
- [9] K. Fukushima and C. Sasaki, *Progress in Particle and Nuclear Physics* **72**, 99 (2013).
- [10] A. Bzdak, S. Esumi, V. Koch, J. Liao, M. Stephanov, and N. Xu, *Physics Reports* **853**, 1 (2020).
- [11] L. Adamczyk et al. (STAR), *Phys. Rev. C* **96**, 044904 (2017).
- [12] B. Abelev et al. (ALICE Collaboration), *Phys. Rev. C* **88**, 044910 (2013).
- [13] B. Abelev et al. (ALICE Collaboration), *Phys. Rev. Lett.* **109**, 252301 (2012).
- [14] A. Andronic, P. Braun-Munzinger, K. Redlich, and J. Stachel, *Nature* **561**, 321 (2018).
- [15] X. Luo, S. Shi, N. Xu, and Y. Zhang, *Particles* **3**, 278 (2020).
- [16] K. Fukushima, B. Mohanty, and N. Xu, (2020), [arXiv:2009.03006 \[hep-ph\]](#).
- [17] A. Bazavov et al. (HotQCD), *Phys. Rev. D* **90**, 094503 (2014).
- [18] O. Kaczmarek, F. Karsch, E. Laermann, C. Miao, S. Mukherjee, P. Petreczky, C. Schmidt, W. Soeldner, and W. Unger, *Phys. Rev. D* **83**, 014504 (2011).
- [19] W.-j. Fu, X. Luo, J. M. Pawłowski, F. Rennecke, R. Wen, and S. Yin, (2021), [arXiv:2101.06035 \[hep-ph\]](#).
- [20] B. Berdnikov and K. Rajagopal, *Phys. Rev. D* **61**, 105017 (2000).
- [21] S. Mukherjee, R. Venugopalan, and Y. Yin, *Phys. Rev. C* **92**, 034912 (2015).
- [22] S. Mukherjee, R. Venugopalan, and Y. Yin, *Phys. Rev. Lett.* **117**, 222301 (2016).
- [23] L. Jiang, S. Wu, and H. Song, *Nucl. Phys. A* **967**, 441 (2017).
- [24] S. Wu, Z. Wu, and H. Song, *Phys. Rev. C* **99**, 064902 (2019).
- [25] M. A. Stephanov, *Phys. Rev. Lett.* **102**, 032301 (2009).
- [26] S. Jeon and V. Koch, in *Quark-Gluon Plasma*, edited by R. C. Hwa and X. N. Wang (2004) p. 430, [arXiv:hep-ph/0304012 \[hep-ph\]](#).
- [27] M. Stephanov, K. Rajagopal, and E. Shuryak, *Phys. Rev. D* **60**, 114028 (1999).
- [28] P. Huovinen, P. Kolb, U. Heinz, P. Ruuskanen, and S. Voloshin, *Physics Letters B* **503**, 58 (2001).
- [29] M. Luzum and P. Romatschke, *Phys. Rev. C* **78**, 034915 (2008).
- [30] C. Gale, S. Jeon, B. Schenke, P. Tribedy, and R. Venugopalan, *Phys. Rev. Lett.* **110**, 012302 (2013).
- [31] H. Song and U. Heinz, *Phys. Rev. C* **77**, 064901 (2008).
- [32] L. Du and U. Heinz, *Computer Physics Communications* **251**, 107090 (2020).
- [33] C. Shen and S. Alzhrani, *Phys. Rev. C* **102**, 014909 (2020).
- [34] D.-U. Jungnickel and C. Wetterich, *Phys. Rev. D* **53**, 5142 (1996).
- [35] V. Skokov, B. Friman, E. Nakano, K. Redlich, and B.-J. Schaefer, *Phys. Rev. D* **82**, 034029 (2010).
- [36] C. D. Roberts and A. G. Williams, *Progress in Particle and Nuclear Physics* **33**, 477 (1994).
- [37] D. U. Jungnickel and C. Wetterich, *Phys. Rev. D* **53**, 5142 (1996).
- [38] B.-J. Schaefer and J. Wambach, *Phys. Part. Nucl.* **39**, 1025 (2008).
- [39] S.-x. Qin, L. Chang, H. Chen, Y.-x. Liu, and C. D. Roberts, *Phys. Rev. Lett.* **106**, 172301 (2011).
- [40] L.-j. Jiang, X.-y. Xin, K.-l. Wang, S.-x. Qin, and Y.-x. Liu, *Phys. Rev. D* **88**, 016008 (2013).
- [41] C. Nonaka and M. Asakawa, *Phys. Rev. C* **71**, 044904 (2005).
- [42] M. A. Stephanov, *Phys. Rev. Lett.* **107**, 052301 (2011).
- [43] L. Jiang, J.-H. Zheng, and H. Stoecker, (2017), [arXiv:1711.05339 \[nucl-th\]](#).
- [44] L. Jiang, P. Li, and H. Song, *Phys. Rev. C* **94**, 024918 (2016).
- [45] L. Jiang, P. Li, and H. Song, *Nuclear Physics A* **956**, 360 (2016), the XXV International Conference on Ultrarelativistic Nucleus-Nucleus Collisions: Quark Matter 2015.
- [46] C. Herold, M. Nahrgang, Y. Yan, and C. Kobdaj, *Phys. Rev. C* **93**, 021902(R) (2016).
- [47] M. Stephanov and Y. Yin, *Phys. Rev. D* **98**, 036006 (2018).
- [48] M. Nahrgang, M. Bluhm, T. Schäfer, and S. A. Bass, *Phys. Rev. D* **99**, 116015 (2019).
- [49] E. Shuryak and J. M. Torres-Rincon, *Phys. Rev. C* **100**, 024903 (2019).
- [50] K. Rajagopal, G. W. Ridgway, R. Weller, and Y. Yin, *Phys. Rev. D* **102**, 094025 (2020).
- [51] M. Bluhm et al., *Nucl. Phys. A* **1003**, 122016 (2020).
- [52] L. Du, U. Heinz, K. Rajagopal, and Y. Yin, *Phys. Rev. C* **102**, 054911 (2020).